

This is the accepted manuscript version of the contribution published as:

Khosrozadeh, S., Guber, A., Kravchenko, A., Ghaderi, N., Blagodatskaya, E. (2022):
Soil oxidoreductase zymography: Visualizing spatial distributions of peroxidase and phenol oxidase activities at the root-soil interface
Soil Biol. Biochem. **167** , art. 108610

The publisher's version is available at:

<http://dx.doi.org/10.1016/j.soilbio.2022.108610>

1 **Soil Oxidoreductase Zymography: Visualizing Spatial**
2 **Distributions of Peroxidase and Phenol Oxidase Activities at**
3 **the Root-Soil Interface**

4 Sajedeh Khosrozadeh^{a,b}, Andrey Guber^{c,d}, Alexandra Kravchenko^c, Negar
5 Ghaderi^a, Evgenia Blagodatskaya^{a,e}

6

7 a Department of Soil Ecology, Helmholtz-Centre for Environmental Research – UFZ, 06120, Halle (Saale), Germany

8 b Department of Soil Science, College of Agriculture, Isfahan University of Technology, 84156-83111, Isfahan, Iran

9 c Department of Soil, Plant and Microbial Sciences, Michigan State University, 48824, East Lansing, MI, USA

10 d DOE Great Lakes Bioenergy Research Center, Michigan State University, 48824, East Lansing, MI, USA

11 e Agro-Technological Institute, RUDN University, 117198, Moscow, Russia

12 **Corresponding Author: Sajedeh Khosrozadeh**

13 Email: s.khosrozadeh@ag.iut.ac.ir

14 Tel: +98 31 33913471

15 Fax: +98 31 33913471

16 Postal address: Department of Soil Science, College of Agriculture, Isfahan

17 University of Technology, 8415683111, Isfahan, Iran.

18

19

20

21 **Abstract**

22 Decomposition of organic material in the rhizosphere – the most dynamic
23 microbial habitat in soil – involves arrays of oxidoreductase and hydrolytic
24 enzymes. Spatial distributions of various hydrolytic activities in soil have
25 already been explored by zymographic techniques. However, the distribution
26 oxidative activity in the rhizosphere remains to be studied. Thus, we extended
27 a Time-Lapse Zymography technique, using Amplex Red[®] reagent, to
28 visualize and quantify distributions of phenol oxidase and peroxidase activities
29 in the rhizosphere of *Zea mays* L. growing in a Haplic Phaeozem and the non-
30 rhizospheric soil. The gross oxidative activity was greatest at the root
31 surfaces, and fell to background soil levels 1.26 and 0.67 mm from seminal (>
32 1 mm diameter) and lateral (<0.5 mm diameter) roots, respectively. The
33 rhizosphere extent relative to the root radius was 55% broader around lateral
34 than around seminal roots. The greatest activities, up to 30 nmol cm⁻² min⁻¹,
35 were peroxidase-dominated and closely associated with roots. The results
36 confirm the utility of the approach for studying spatio-temporal distributions of
37 oxidative activities in soil. However, actual activity of oxidoreductases in the
38 field will be strongly controlled by fluctuating environmental conditions such as
39 soil aeration and the gradient of reactive oxygen species, which need to be
40 considered especially in anoxic soils.

41 **Keywords:** Amplex Red, Soil oxidative activity, Peroxidase and phenol
42 oxidase, Spatial distribution, Time-Lapse Zymography.

43 **Abbreviations:** ABTS, 2,2'-azino-bis (3-ethylbenzthiazoline-6-sulfonic acid);
44 AMC, 7-amino-4-methylcoumarin; Amplex Red[®] reagent, 10-acetyl-10H-

45 phenoxazine-3,7-diol (ADHP); GSV, greyscale value; MUF, 4-
46 methylumbelliferone; TLZ, Time-Lapse Zymography; RMSE, root mean
47 square error; SD, standard deviation.

48 **Highlights**

- 49 • A Time-Lapse Zymography technique was developed for soil
50 oxidoreductases.
- 51 • Oxidative activity in the maize rhizosphere was dominated by peroxidases.
- 52 • The relative rhizosphere extent was broader around lateral (thin) than
53 around seminal (thick) roots.

54 **1. Introduction**

55 The root-soil interface is a highly dynamic habitat, in which diverse
56 microbial processes are driven by easily degradable organic compounds
57 secreted by roots into the rhizosphere (Kuzyakov, 2002; Hinsinger et al.,
58 2009). Rhizodeposits influence organic matter cycling by stimulating microbial
59 growth and production of exo-enzymes that facilitate decomposition of
60 numerous organic compounds (Dwivedi et al., 2019). Highly diverse
61 oxidoreductase and hydrolytic enzymes — actively secreted by bacteria,
62 fungi, and living roots — are responsible for catalyzing decomposition of these
63 organic composites (Dennis et al., 2010; Theuerl and Buscot, 2010; Burns et
64 al., 2013). The first stage of decomposition begins with oxidative processes
65 mediated by multiple oxidoreductases (Sinsabaugh, 2010; Burns et al., 2013),
66 which are mostly present in the vicinity of roots, microbial cells, and
67 decomposing components (Gramss et al., 1999; Tuomela and Hatakka,
68 2011). Despite the multi-functional roles of oxidoreductases in transformation

69 of soil organics, little is known about their distribution in rhizosphere and non-
70 rhizospheric soil. This is partly because previous zymographic attempts to
71 visualize distributions of enzymatic activities in soil have focused on hydrolytic
72 reactions (Spohn et al., 2013; Sanaullah et al., 2016).

73 Oxidative processes in soil are catalyzed by oxidoreductases, generally
74 categorized as phenol oxidases and peroxidases (Sinsabaugh, 2010; Burns et
75 al., 2013). These enzymes non-specifically catalyze cleavage of links in
76 electron-rich substrates (e.g., phenols, lignin, thiols, aromatic alcohols and,
77 unsaturated lipids) across a wide range of redox potential (German et al.,
78 2011; Tuomela and Hatakka, 2011), which is crucial for decomposition of
79 diverse biotic and xenobiotic aromatic compounds in soil (Gramss et al., 1999;
80 Muratova et al., 2009). Studies on oxidoreductases in soil have mainly
81 focused on the degradation of lignin and bioremediation of aromatic
82 compounds, while the oxidoreductases have multiple physiological functions
83 including morphogenesis, cell metabolism, protective function in pathogenic-
84 plant interactions and under stress conditions (Courty et al., 2009). Phenol
85 oxidases — copper metalloenzymes that typically have four copper (Cu)
86 atoms in their interaction centers — catalyze the degradation of phenolic
87 compounds by reducing molecular oxygen to water (Bach et al., 2013).
88 Laccases are the most intensively investigated phenol oxidases in soil. They
89 are encoded by multigene families and produced by bacteria, fungi, and
90 plants, so laccases with vast functional diversity participate in decomposition
91 processes (Theuerl and Buscot, 2010; Burns et al., 2013). Numerous phenols,
92 aromatic amines, and heterocyclic compounds can be oxidized by laccases.
93 However, oxidation is usually restricted by the low redox potential of laccases

94 (450 – 800 mV). For example, they cannot directly oxidize non-phenolic bonds
95 in lignin with a redox potential over 1500 mV (Tuomela and Hatakka, 2011;
96 Bach et al., 2013). In contrast, peroxidases have sufficiently high redox
97 potential, up to 1490 mV (Bach et al., 2013), to cleave aryl and alkyl bonds in
98 lignin (Tuomela and Hatakka, 2011). Members of the peroxidase superfamily
99 (e.g., horseradish, lignin, and manganese peroxidases) are heme-containing
100 glycoprotein enzymes that require H₂O₂ (instead of oxygen) as an electron
101 acceptor to oxidize phenolic compounds (Sinsabaugh, 2010; Burns et al.,
102 2013).

103 A fluorometric microplate technique has been developed for assaying
104 laccases activities in homogenized soil suspensions, which are assumed to
105 be representative for overall oxidative activities, using Amplex Red as a
106 substrate (Wang et al., 2017). Peroxidases require H₂O₂ for activity, but not
107 phenol oxidases. Therefore, substrate oxidation rates determined in the
108 presence and absence of H₂O₂ respectively correspond to activities of both
109 enzymes and solely phenol oxidase activities. Thus, peroxidase activities can
110 be simply estimated from differences between rates measured with and
111 without H₂O₂ (Sinsabaugh, 2010; Bach et al., 2013; Burns et al., 2013).
112 However, microplate assays do not provide information on the localization of
113 oxidative processes in soil (German et al., 2011). The rhizosphere
114 encompasses peroxidases and phenol oxidases originating from both
115 microbes (soil- and root-associated) and plants (Gramss et al., 1999;
116 Cheeseman, 2007). As enzymes secreted by plants and root-associated
117 microbes do not diffuse in a long distance away from roots (Guber et al.,
118 2018; Kuzyakov and Razavi, 2019), the oxidative processes are expected to

119 be more intensive at root surfaces and in the rhizosphere than in bulk soil
120 (Criquet et al., 2000; Muratova et al., 2009). However, such an assumption
121 still requires experimental proof by estimation of localized oxidoreductase
122 activities at root-soil interfaces.

123 The two-dimensional distribution of hydrolytic enzyme activities in
124 undisturbed soil have been visualized by zymographic techniques in which
125 fluorescent dye-conjugated substrates such as 4-methylumbelliferone (MUF)
126 or 7-amino-4-methylcoumarin (AMC) are integrated (Spohn et al., 2013;
127 Spohn and Kuzyakov, 2013; Sanaullah et al., 2016). With appropriate
128 modification, the technique enables visualization of activities of diverse
129 hydrolytic enzymes, such as proteases, amylases (Spohn et al., 2013), acid
130 and alkaline phosphatases (Spohn and Kuzyakov, 2013), β -glucosidases
131 (Sanaullah et al., 2016), cellobiohydrolases, leucine aminopeptidases,
132 xylanases, and chitinases in various soil hotspots including rhizosphere,
133 detritusphere, and biopores (Hoang et al., 2016; Loepmann et al., 2016; Ma
134 et al., 2018). However, zymographic techniques using labelled-fluorogenic
135 substrates have not been previously applied successfully to oxidoreductases,
136 despite their importance in organic matter transformation in the rhizosphere
137 and at soil surfaces. Recent attempts to develop a zymographic technique for
138 phenol oxidases using 2,2'-azino-bis (3-ethylbenzthiazoline-6-sulfonic acid;
139 ABTS), have revealed several methodological restrictions, including lack of
140 calibration of the oxidized product of ABTS (which is not commercially
141 available), low sensitivity, and interference from light adsorption by soil
142 minerals and organic matter (Leue et al., 2021). As the end product of ABTS
143 assay is not readily synthesized (Leue et al., 2021), purified laccases or

144 horseradish peroxidases were used for calibration to transform ABTS to the
145 oxidized product (German et al., 2011). The assumption of this method is that
146 initial ABTS concentration equals to the concentration of oxidized product. If
147 this assumption is not valid, the calibration coefficient will be incorrect
148 (German et al., 2011). Therefore, the commercial oxidized product of ABTS
149 with known concentration is necessary to accurately measure enzyme activity.
150 It is anticipated that much better results could be obtained using a fluorescent
151 reagent for zymographic analysis of oxidative enzymes.

152 In fluorogenic zymography, a membrane saturated with an enzyme-specific
153 fluorogenic substrate is placed on the surface of soil, and decomposition of
154 the substrate catalyzed by enzymes in the soil is monitored (Razavi et al.,
155 2019). A fluorescent product appears in the membrane due to diffusion of the
156 substrate from the membrane to the soil, its cleavage by enzymes and
157 diffusion of the product back to the membrane (Guber et al., 2018). The
158 distance between the membrane and enzymes affects the diffusion length and
159 time, manifested in non-linear signal development in the membrane (Guber et
160 al., 2018; Guber et al., 2021). Thus, an approach called Time-Lapse
161 Zymography (TLZ) methodology was recently developed by Guber et al.
162 (2021) to account for the signal non-linearity and diffusion losses of the
163 product in the activity calculations, thereby providing more accurate estimates
164 of enzyme activities than traditional membrane zymography (Spohn et al.,
165 2013; Sanaullah et al., 2016).

166 The aim of the study presented here was to extend TLZ methodology to
167 oxidoreductases. For this, we used Amplex Red, which forms the brightly
168 fluorescent product resorufin when oxidized (Zhao et al., 2012). Amplex Red

169 has been used for imaging locations of reactive oxygen species (particularly
170 H₂O₂) that may appear at shoot apices and root surfaces (Driever et al., 2009;
171 Kováčik et al., 2014; Voothuluru et al., 2018; Huang et al., 2020), as well as
172 for measuring enzyme activities in soil suspensions (Wang et al., 2017). It has
173 also been used to measure extracellular H₂O₂ concentrations and peroxidase
174 activities in organelles and tissues (Reszka et al., 2005), and thus has
175 apparent utility as a fluorogenic substrate for zymographic visualization of
176 oxidative enzyme activities. Moreover, resorufin can be easily quantified,
177 thereby enabling straightforward calibration of oxidoreductase activities. Thus,
178 we tested the applicability of Amplex Red-based zymography to quantify and
179 visualize localizations of oxidative processes in non-rhizosphere and
180 rhizosphere soil of maize (*Zea mays* L.). We also tested its ability to
181 distinguish between activities of phenol oxidases alone (in the absence of
182 H₂O₂) and both peroxidases and phenol oxidases (in the presence of H₂O₂).
183 We hypothesized that oxidoreductase activities are greater in the rhizosphere
184 than in non-rhizospheric soil.

185 **2. Materials and Methods**

186 *2.1 Soil sampling and preparation*

187 Soil used within the framework of the Priority Program 2089 “Rhizosphere
188 spatiotemporal organization – a key to rhizosphere function”, was collected
189 from an agricultural crop rotation plot in September 2018 from a 0–50 cm
190 layer of loamy Haplic Phaeozem planted with oilseed rape (Vetterlein et al.,
191 2021) near Schladebach, Saxony-Anhalt, Germany (51.3087° N, 12.1045°E).
192 The soil had the following physicochemical characteristics: 33% sand, 48%

193 silt, and 19% clay, 8.6 g kg⁻¹ total organic C content, 0.84 g kg⁻¹ total N
194 content, 10.2 C:N ratio and, pH (CaCl₂) of 6.4. The soil and sampling
195 procedure are described in more detail by Vetterlein et al. (2021). After
196 sampling, the soil was air-dried, sieved to a particle size of ≤2 mm, and stored
197 at room temperature.

198 *2.2 Experimental setup and plant growth conditions*

199 Soil and seeds were prepared as described by Vetterlein et al. (2021). The
200 soil was fertilized with 50 mg N (NH₄NO₃), 50 mg K (K₂SO₄), 25 mg (MgCl₂
201 6H₂O), and 40 mg P (CaHPO₄) per kg dry mass and passed through a ≤1 mm
202 sieve to evenly distribute the fertilizer. The sieved soil was packed in three
203 replicated rhizoboxes (3×8.8×17.8 cm, H×B×L; Clickbox[®] Germany) to a final
204 bulk density of 1.26 g cm⁻³. The Maize (*Zea mays* L.) was selected as a model
205 plant, because maize roots produce considerable amount of oxidoreductases
206 contributing in lignin polymerization and the oxidative degradation of organic
207 compounds in soil (Gramss et al., 1999). Maize (*Zea mays* L.) seeds were
208 surface-sterilized for 10 min in 10% H₂O₂ solution, kept for 5 min in H₂O, and
209 soaked in saturated CaSO₄ solution for 3 h. The seeds were then sown 1 cm
210 below the soil surface in three rhizoboxes and covered with a layer of fine
211 gravel (4 – 8 mm) to reduce water losses through evaporation. The rhizobox
212 walls were covered with aluminum foil to prevent algal growth. Throughout the
213 growth period (60 days) a soil water content of 22% (v/v) was maintained in
214 the rhizoboxes, which were inclined at 50° during the experiment to direct root
215 growth along their lower (front) panels. The rhizoboxes were weighed every
216 day and the lost weight was compensated by distilled water. The design of the

217 rhizoboxes simulated the situation of a well aerated soil and the roots were
218 exposed to air as the rhizoboxes were designed with an opening front panel.

219 *2.3 Soil zymography*

220 The TLZ approach (Guber et al., 2021) was used for the oxidative
221 zymography. A stock substrate solution was obtained by dissolving 25 mg of
222 Amplex Red[®] reagent (10-acetyl-10H-phenoxazine-3,7-diol (ADHP); CAS
223 Number: 119171-73-2; highly sensitive probe for H₂O₂ and fluorogenic
224 substrate for peroxidase assay with commercial names Amplex Red,
225 Ampliflu[™] Red, and Oxi red) in 1 ml of dimethyl sulfoxide (DMSO) then
226 diluting in deionized water to an Amplex Red concentration of 50 mM. The
227 stock solution was further diluted in 50 mM Trizma buffer (pH 7.4) to obtain a
228 2 mM working solution of the substrate. Inert gas (N₂) was bubbled through
229 the working solution, in a glass vial for 5 min, keeping the lid tightly closed
230 thereafter. The solutions were prepared in a dark room, and all glasses used
231 were covered by aluminum foil to prevent substrate photo-oxidation. Two 6 ×
232 8 cm hydrophilic polyamide membrane filters, 100 μm thick with 0.45 μm pore
233 sizes (Tao Yuan, China), were soaked in the Amplex Red working solution for
234 3 minutes. Immediately before soaking the membrane, a 0.3% H₂O₂ solution
235 was added to Amplex Red working solution, at an Amplex Red - to - H₂O₂
236 volume ratio of 1:10. The membrane saturated by this solution was used for
237 measurements of gross phenol oxidase and peroxidase activities. The other
238 membrane was saturated in Amplex Red substrate with no H₂O₂ addition to
239 determine solely phenol oxidase activity. The rhizoboxes were opened from
240 the root side and placed in a dark chamber with 15 W blue-black ultraviolet
241 lamps - (erolite[®] Germany) as sources of UV light. The saturated membranes

242 were placed directly on the soil-root surfaces for zymographic imaging
243 (focusing on the developed branched root parts containing seminal and lateral
244 roots). Two membranes (with and without H₂O₂ treatments) were placed
245 simultaneously in the same replicated rhizobox at the areas with similar root
246 density, i.e., 6 membranes in total. To measure enzymatic activity, the mean
247 values for the whole membrane were assessed. Mean activity of individual
248 membrane was considered as a true replicate of each rhizobox. The average
249 values were calculated by corresponding mean activities of three rhizoboxes.
250 A transparent glass sheet was placed over the membranes to keep them in
251 contact with the soil and prevent from direct contact to room air and
252 evaporation of the substrate from the membranes during the zymography. A
253 D3500 DSLR camera with AF-P DX NIKKOR 18-55 mm f/3.5-5.6G VR lens
254 (Nikon Inc.), was used to capture images. The focal length, aperture, and
255 shutter speed were set to 210 mm, f/6.3, and 1/125 s, respectively. The
256 camera settings, the distance between the sample and the source of UV light
257 were fixed to obtain time-series of images of the membranes at 28 μm pixel⁻¹
258 resolution: 0, 5, 10, 15, 20, 30, 60 and, 90 minutes after placing them on the
259 soil-root surface.

260 Calibration standards were prepared to convert the brightness of the image
261 pixels to resorufin content equivalents, as follows. A 1 mM resorufin (7-
262 hydroxy-3*H*-phenoxazin-3-one sodium salt, C₁₂H₆NNaO₃) stock solution was
263 prepared by dissolving resorufin in 50 mM Trizma buffer (pH 7.4). The stock
264 solution was further diluted in the Trizma buffer to obtain 0.2, 0.4, 0.6, 0.8,
265 and 1-mM calibration solutions. To validate the calibration 0.1, 0.3, 0.5, 0.7
266 and 0.9 mM resorufin solutions were prepared in the same way as the

267 calibration solutions. To protect the resorufin solutions from degradation by
268 light, the standard solutions were prepared in a dark room and all flasks were
269 covered by aluminum foil. A 10 μ l portion of each calibration and validation
270 solutions was added to membranes (12 \times 8.5 cm; to image the range of
271 resorufin concentrations simultaneously), which were then covered by a
272 transparent glass sheet to mimic the zymography settings. The membranes
273 with standards were photographed under UV light using the same camera
274 settings as for the TLZ. Due to sensitivity of Amplex Red and resorufin to
275 high-energy light, the rhizoboxes and calibration membranes were covered
276 between the TLZ imaging.

277 *2.4 Image processing*

278 The calibration images were used to determine the relationship between
279 image brightness and resorufin contents in image pixels. We first extracted
280 red channel signals from the images using the “Split Channels” tool of the
281 ImageJ software (Schindelin et al., 2012) and converted the resulting images
282 to 8-bit format without rescaling. Then we adjusted the 8-bit images to
283 account for background brightness by subtracting average greyscale values
284 (GSVs) of the calibration images with zero concentration of resorufin, and
285 counted numbers of pixels in the GSV range (0 - 254) in the resulting images
286 using ImageJ’s “Analyze histogram” tool. Following Guber et al. (2019) a
287 calibration coefficient (a) was calculated from linear regression of applied
288 resorufin amount (nmol/10 μ l) against GSV sums in the calibration images as:

$$289 \quad M_i = a \sum_1^n G_i^j F_i^j \quad 1 < j < 255 \quad (1)$$

290 Where: M_i is the applied amount of resorufin in calibration solution i [nmol]; G_i^j
291 and F_i^j are the GSV and number of pixels for bin j in the greyscale histogram
292 at i -concentration [nmol] and [pix], respectively; and a is the conversion
293 coefficient from G_i^j to the mass of resorufin in image pixels [nmol greyscale
294 value⁻¹ pixel⁻¹].

295 The calibration accuracy was assessed for both calibration and validation
296 datasets using the Root-Mean-Square-Error (RMSE):

$$297 \quad RMSE = \sqrt{\frac{1}{N} (M_c - M_i)^2} \quad (2)$$

298 where M_c is the amount of resorufin calculated using Eq. (1) for i -
299 concentration [nmol].

300 The time series of oxidized zymography images were processed using the
301 protocol described by Guber et al. (2021) to obtain the enzyme activity images
302 (zymograms). Analyses of time series of GSV in image pixels revealed two
303 clear linear phases, in the 0-15- and 30-90-min intervals (Fig. 3), so
304 zymograms were calculated separately for each of these intervals in the
305 zymography sequences.

306 *2.5 Image analysis*

307 Zymograms of gross oxidative activity were analyzed to assess differences
308 in activities between root areas, hotspots, and non-rhizospheric soil. The extent
309 of the rhizosphere around roots of varying thickness was also assessed. To do
310 that the root daylight images were combined with zymograms. The root
311 locations on zymograms were derived from the rhizobox images taken at day
312 light shortly before zymography. The rhizobox images were converted to 8-bit

313 format, binarized using the Otsu thresholding tool, and the resulting images (of
314 roots) were super-imposed on the oxidative zymograms. Only the areas where
315 the membrane was in direct contact with the root/soil surface were included in
316 the analyses (Fig. 4; the rectangles on the daylight image showed the examples
317 of good and bad attachment). Autofluorescence of soil particles (if any) was
318 avoided by an attachment of the membrane, which did not show noticeable
319 autofluorescence. In addition, it is easy to distinguish the oxidative activity and
320 auto-fluorescence of soil particles by colour. In Amplex Red assay, the resorufin
321 signal (oxidized product of Amplex Red) is emitted at 530 – 575 nm and its
322 fluorescence signal under UV light is red (Zhao et al., 2012). While, the auto-
323 fluorescence of soil organic particles is emitted at 350 – 470 nm (Tang et al.,
324 2019), and its fluorescent colour under UV light is blue. There is no interference
325 between soil particles auto-fluorescence and resorufin signal.

326 Enzyme activities were analyzed using ImageJ's Plot Profile tool in cross-
327 sections drawn across selected seminal (thick, larger than 1 mm) and lateral
328 (thin, smaller than 0.5 mm) roots (Hochholdinger, 2009) perpendicular to their
329 axes. The reason for choosing lateral and seminal roots was to prove that
330 both young and relatively aged roots have great potential of oxidative
331 reaction. Three roots of each type (lateral and seminal) were selected in each
332 zymogram with H₂O₂ membrane (18 roots in total). The membranes without
333 H₂O₂ were not considered due to overall low root zone activity in the absence
334 of H₂O₂. The mean values of each rhizobox were considered as true
335 replicates. The average values were calculated by corresponding mean
336 rhizosphere extensions of three rhizoboxes. The root zones were defined in
337 the Profile plots using the root daylight images. The rhizosphere extents were

338 identified by analyzing activity histograms in root and non-rhizosphere soil on
339 the oxidative zymograms. The average GSVs histograms of oxidative activity
340 in non-rhizosphere soil area was defined as the mean soil activities.
341 Rhizosphere extents were then estimated by determining a distance between
342 a region with upper levels of activities in the soil (estimated by each of several
343 methods explained in Table 1; e.g., 20%, 30% or SD higher than soil activity)
344 and root center (Fig. 1A). The distribution of 'hotspots' was estimated
345 according to Bilyera et al. (2020), as explained in Table 1 and Fig. 1B. A
346 normal distribution was fitted to the low range of enzyme activities in the
347 histogram that included both root and soil areas in the zymograms (Fig. 1B).
348 The mean GSV + two standard deviations (2SD) of the fitted distribution was
349 considered as soil background activity, and was thus removed from the
350 activity image to identify the hotspots.

351 *2.6 Statistical analysis*

352 The differences between the treatments in terms of oxidative activity were
353 analyzed using PROC MIXED procedure in SAS (SAS Institute, 2013). The
354 statistical model included H₂O₂ treatment (present, absent and subtraction
355 between them), the study area (soil and root), and the time interval (0-15 and
356 30-90 min) as the studied fixed factors and their two- and three-way
357 interactions. The model also included the random effect of rhizobox replicates
358 and the random effect of the membrane (expressed as the interaction
359 between the rhizobox and H₂O₂ treatment) which was used as an error term
360 to test the effect of the H₂O₂ treatment. In addition, the random effect of the
361 study area within the membrane (expressed as the interaction between the
362 rhizobox, H₂O₂ treatment, and study area) was used as an error term to test

363 the effect of the study area. Normal probability plots of the residuals showed
364 that assessment of the normality assumption was violated, so the data were
365 log-transformed. The three-way interaction was subjected to slicing, also
366 known as simple effect tests. Mean values within slices for which F-tests
367 indicated there were significant differences at $P < 0.05$ were compared using
368 t-tests. The significance of differences in rhizosphere extent between seminal
369 (thick) and lateral (thin) roots was assessed using Tukey's test ($P < 0.05$). All
370 figures were prepared with R version 4.0.3 (R Development Core Team,
371 2020) in the R Studio.

372 **3. Results**

373 GSV sums in the calibration and validation images linearly correlated with
374 applied amount of resorufin within the range 2 - 10 nmol ($R^2 = 0.997$, Fig. 2).
375 The value of the calibration parameter a was 2.45×10^{-7} nmol greyscale⁻¹ pix⁻¹,
376 and RMSE values for the calibration and validation datasets were 0.094 and
377 0.035 nmol, respectively, indicating that the calibration was robust.

378 The signal in the membranes developed linearly with time during first 15–
379 20 min (Fig. 3). Both with and without H₂O₂ the slopes of the GSV time series
380 were much steeper (and hence corresponding changes in enzyme activities
381 were greater) during the first 15 minutes than during the 30–90 minutes
382 interval (Fig. 3). The stability of fluorescent signal of resorufin on the
383 calibration membranes has been tested experimentally and it was relatively
384 stable during experiment according to the similar slopes of the calibration
385 lines obtained at different time intervals (Fig. S1).

386 The enzyme activities were also much greater in the presence of H₂O₂ in
387 the substrate (Fig. 4Aa) than in its absence (Fig. 4Ba). The intensity and
388 distribution of fluorescent signal varied between replicated rhizoboxes (Fig.4
389 Aa, S2 Ca, S2 Ea). In general, however, during the first 15 minutes of TLZ the
390 activities were greater in the root zones than in the soil in the presence of
391 H₂O₂ (Fig. 4Aa), but greater in the soil than the root zones in its absence (Fig.
392 4Ba). The same patterns were observed, albeit less prominently, during the
393 30–90 minutes interval (Fig. 4Ab and Bb). Remarkably, some roots had no
394 apparent oxidative activity, even in the presence of H₂O₂, despite being alive
395 and clearly visible. This can be associated either with the absence of enzyme
396 activity or with poor contact between the membrane and soil/root surface (as
397 illustrated as an example by the red rectangles in Fig. 4Aa and Ac).

398 The gross oxidative activity was not evenly distributed between phenol
399 oxidases and peroxidases. During the first 15 minutes of TLZ, peroxidase
400 activity was 26 times greater at the root surface as compared to the non-
401 rhizosphere soil (Fig. 5). The observed trend markedly differed during the 30–
402 90 minutes TLZ interval, when activities of both enzymes were greater by the
403 roots than in the non-rhizosphere soil (Fig. 5). Despite the numerical
404 differences between activities of the two enzymes, the differences in averaged
405 values were only significant for peroxidase ($P < 0.05$) at the root surface
406 during the 0–15 minutes TLZ interval (Fig. 5).

407 The gross oxidative activity, measured with H₂O₂ in the substrate, gradually
408 decreased with distance from the center of both thick (seminal) and thin
409 (lateral) roots towards surrounding soil (Fig. 6A and 6B). However, root

410 thickness affected the oxidative activity distribution patterns. Specifically, the
411 oxidative activity was approximately 20% greater on the surface of thick
412 (seminal) than on the surface of thin (lateral) roots, and the hotspot areas
413 were up to 1.8 times broader around the thick (seminal) than around the thin
414 (lateral) roots. The rhizosphere, defined in terms of gross oxidative activity,
415 was on average 42% broader around seminal (thick) roots than around lateral
416 (thin) roots, extending 1.26 and 0.73 mm from their centers, respectively (Fig.
417 6C). However, the rhizosphere extents normalized by the root thickness were
418 nearly 2.4 times broader for thin (lateral) than for thick (seminal) roots (Fig.
419 6D). The listed calculation methods (Table 1) yielded extents that declined in
420 the following order: soil mean value +20% > soil mean value + 30% > soil
421 mean value + SD > soil mean value + 2SD (hotspots). The soil mean value +
422 20% yielded 6% broader rhizospheres than soil mean value + SD (Table 1). In
423 the presence of H₂O₂, the 'hotspot areas' estimated according to Bilyera et al.
424 (2020), were on average 8% and 13% narrower than the 'rhizosphere areas'
425 (defined as areas with soil mean values + 1 SD) of the thick (seminal) and thin
426 (lateral) roots, respectively (Fig. 6A and B). In contrast, in the absence of
427 H₂O₂ the enzyme activity was weaker at the root surfaces than in the soil.

428 **4. Discussion**

429 *4.1 Resorufin-based calibration and validation*

430 The correlation between GSV sums and resorufin amount in the calibration
431 membranes (Fig. 2) enabled linear calibration of phenol oxidase and
432 peroxidase activities using commercially available resorufin. This has three
433 advantages over the traditional calibration approach, involving use of
434 membranes uniformly saturated in MUF solutions with a range of

435 concentrations (Spohn et al., 2013). First, due to the radial diffusion of the
436 applied calibration solution within the membrane, each calibration/validation
437 membrane provides a range of resorufin concentrations with different GSV in
438 individual pixels within the application areas. Therefore, each datapoint along
439 the regression line defined by Eq. 1 and shown in Fig. 2 represents GSV
440 recorded in a substantial number of pixels (approximately 3.5×10^4). Second,
441 use of a validation dataset with different spatial distributions of the
442 concentrations within application areas provides confidence in the robustness
443 of the calibration equation and reliability of its parameter. Third, in contrast to
444 calibration of hydrolytic activity by MUF (Guber et al., 2019; Hummel et al.,
445 2021), we did not observe brightness saturation of the fluorogenic signal,
446 which enabled linear calibration across the whole range of applied
447 concentrations.

448 *4.2 Time-lapse zymography*

449 Despite the fluorescence signals gradually increasing until the end of the
450 90-minute course of zymography (Fig. 3, 4Bb, and S1), increases in GSV
451 (and hence oxidative activities) with time appeared to be greatest during the
452 0–15 minutes interval (Fig. 3). The considerably lower rate of signal increases
453 during the 30–90 minutes interval was likely due to losses of resorufin for
454 diffusion and the substrate concentration in the membrane falling below the
455 threshold required for maximum production (Guber et al., 2018). Diffusion of
456 fluorogenic substrate and products of enzymatic reactions within the
457 membrane and soil matrix causes blurring of zymographic images and
458 reduces the accuracy of hydrolytic or oxidative activity calculations. Our
459 results clearly demonstrate the ability of the time-lapse approach to mitigate

460 the diffusion problem associated with oxidative zymography, as it accounts for
461 resorufin losses through diffusion and enables choice of an appropriate time
462 interval with a steep linear increase in fluorescent signal. The linear increase
463 in resorufin levels within 15 minutes of zymography observed in this study
464 (Fig. 3) enables more accurate calculations, with less risk of underestimating
465 oxidative activity, than traditional zymographic analysis of hydrolytic enzyme
466 activities based on acquisition of single images in the 30–60 minutes (Spohn
467 and Kuzyakov, 2013; Ma et al., 2018). The feasibility of the short zymography
468 time (15 min) was confirmed by the stability of the resorufin calibration lines
469 during zymography (Fig. S1) and the linear increase in the fluorescence signal
470 of the oxidation product of Amplex Red (Fig. 3). This is a clear advantage of
471 the determination of oxidative activities over determination of hydrolytic
472 activities, permitted by the very fast (within several minutes) oxidation of
473 Amplex Red.

474 The fast evolution of a zymographic resorufin signal resulting from Amplex
475 Red oxidation is consistent with findings by Lefrançois et al. (2016) that
476 electrochemical generation of resorufin (by applying +0.50 V vs. Ag/AgCl)
477 resulted in a fluorescent signal within 10 minutes. Our recommendation for
478 short oxidative zymography (e.g., 10-15 minutes) is in line with
479 recommendations to use short incubation times (e.g., 10 minutes) for
480 assaying activities of laccases (Wang et al., 2017) in soil. Moreover, as
481 Amplex Red is sensitive to visible/UV light, increasing oxidative zymography
482 durations (i.e., exceeding 15 min) with exposure of the substrate and product
483 to a high-energy light source (UV-lamp) in the presence of electron acceptor
484 (e.g., H₂O₂, O₂) might have two opposing consequences. One is artificial

485 reduction by transformation of resorufin (oxidation product) to non-fluorescent
486 dihydroresorufin (Lefrançois et al., 2016). The other is generation of resorufin
487 signals by Amplex Red photo-oxidation (Zhao et al., 2012), and hence
488 inaccurate estimation of oxidative activity. In the presence of oxygen and
489 high-energy light, resorufin was converted into dihydroresorufin (photo-
490 bleaching process), while the reverse oxidation reaction was no longer
491 occurred when the light was turned off (Zhao et al., 2011). Thus, to minimize
492 exposure of the Amplex Red and product (resorufin) to high-energy light we
493 conducted the experiment in a dark room and covered the rhizoboxes'
494 surfaces between TLZ intervals.

495 *4.3 Distribution of oxidative activity*

496 The high oxidative activity at the surface of thick (seminal) roots of maize
497 (Fig. 4Aa, shown by blue dashed rectangles) may be associated with
498 increases in production of lignin-like compounds in mature root tissues. This is
499 because the polymerization of lignin precursors is mediated by peroxidases.
500 Peroxidases superfamily in the presence of H₂O₂ can oxidize phenolic
501 compounds and regulate the polymerization of lignin and suberin by root
502 ageing (Dragišić Maksimović et al., 2008). Oxidative activity observed around
503 the thin (lateral) roots (Fig. 4 Aa, shown by yellow dashed rectangles) was
504 likely associated with the protection against excessive generation of reactive
505 oxygen species provided by peroxidases during root cell proliferation (Csiszár
506 et al., 2012). However, oxidative activities were more intense and hot-spots
507 were more concentrated in the vicinity of thick (seminal) roots than in the
508 vicinity of thin (lateral) roots, where they were more homogeneously spread
509 around the roots (Fig. 4Aa). This is consistent with expectations that root

510 growth and turnover affect the production of oxidative enzymes and many
511 associated processes, including lignin synthesis, degradation of phenolic
512 compounds, cell proliferation, root elongation, and protection (Dragišić
513 Maksimović et al., 2008; Csiszár et al., 2012). The enzymes responsible for
514 the greater oxidative activities in the rhizosphere than in non-rhizospheric soil
515 presumably originate from either the plant roots or root-associated
516 microorganisms. This is because the diffusion of enzymes in soil is limited by
517 their high molecular weight (Guber et al., 2018; Kuzyakov and Razavi, 2019)
518 and short half-lives (Burns, 1982; Nannipieri et al., 2002). Sources of oxidative
519 enzymes in or from plant roots include epidermal cells, cell walls and
520 exudates (Gramss et al., 1999). The presence of H₂O₂ as a reactive oxygen
521 species in the cells (e.g., plant root cell) can stimulate the activity of
522 peroxidases (Huang et al., 2020; Cheeseman, 2007) that use H₂O₂ as an
523 electron acceptor in oxidization of phenolic compounds (Dragišić Maksimović
524 et al., 2008). In addition, labile organics exuded by roots and dead root
525 tissues containing phenolic compounds promote increases in microbial
526 abundance in the rhizosphere (Hinsinger et al., 2009; Dennis et al., 2010).
527 Thus, root-associated bacteria and mycorrhizae exploit oxidative enzymes in
528 the decomposition of organic substrates in the rhizosphere (Criquet et al.,
529 2000). For instance, oxidative decomposition mechanisms are stimulated in
530 the presence of carbon sources provided by host plants to ectomycorrhizal
531 fungi (Shah et al., 2016). Stimulation of microbial oxidative enzyme activity by
532 N-containing root exudates also accelerates nitrogen mineralization in the
533 rhizosphere (Zhu et al., 2014). As with hydrolytic exoenzymes, it is not

534 possible to distinguish between the plant or microbial origin of the activity of
535 oxidative enzymes in the rhizosphere.

536 Peroxidases accounted for up to 90% of gross oxidative activity at the root
537 surfaces (Fig. 5), in accordance with reports that they are the main oxidative
538 systems in roots (Gramss et al., 1999) and their exudates (Dragišić
539 Maksimović et al., 2008; Muratova et al., 2009). In non-rhizosphere soil,
540 however, the dominance of peroxidase activity was not statistically confirmed
541 and the essential contribution of phenol oxidases to the total activity cannot be
542 fully excluded (Fig. 5). Many widespread fungi and some bacteria (e.g.,
543 actinomycetes, α -proteobacteria, and γ -proteobacteria) in soil can degrade
544 various recalcitrant aromatic compounds (e.g., lignin, humic substance) by
545 producing highly efficient oxidative enzymes such as laccases grouped as
546 phenol oxidases (Baldrian, 2006; Bugg et al., 2011). These decomposition
547 processes occur outside the cells due to high molecular weights of the
548 substrates (Tuomela and Hatakka, 2011). Therefore, the distribution of phenol
549 oxidases in soil might be associated with microbial activity.

550 *4.4 Comparison of oxidative and hydrolytic zymography*

551 We detected up to three times greater mean oxidative activity in the maize
552 rhizosphere than in non-rhizospheric soil (Fig. 4). This rhizospheric effect on
553 oxidative activity was 1.3–2 times greater than effects estimated
554 zymographically for hydrolytic enzymes including β -glucosidase (Sanaullah et
555 al., 2016), β -cellobiohydrolase, β -xylosidase, and leucine aminopeptidase
556 (Loeppmann et al., 2016; Ma et al., 2018). The spatial distribution of oxidative
557 activity (Fig. 6A and B) was similar to the generally observed decrease in

558 activity of hydrolytic enzymes with distance from plant roots (Kuzyakov and
559 Razavi, 2019). The rhizosphere extent of oxidative activity of thick seminal
560 (1.26 mm) and thin (0.73 mm) lateral roots was on average lower or within the
561 lower part of the range (1–3 mm) estimated for most hydrolytic enzymes (Ma
562 et al., 2018; Kuzyakov and Razavi, 2019). The smaller rhizosphere extent
563 obtained in this study can be partly attributed to the difference in image
564 processing by TLZ and traditional zymography, as well as the shorter
565 zymography duration (15 and 30–60 min, respectively). The former reduces
566 the biases related to radial diffusion of the product within the membrane from
567 enzymatically active zones during the oxidative zymography. In contrast,
568 longer duration of hydrolytic zymography, can clearly lead to overestimates of
569 rhizosphere extent (Guber et al., 2021). The complex dependence of oxidative
570 activities of plant root and associated microorganisms on the abundance of
571 enzymes, reactive oxygen species, and production of phenolic compounds in
572 the rhizosphere also presumably contributed to the differences between
573 rhizosphere extents determined for oxidative and hydrolytic enzymes. Despite
574 they are relatively narrow, the zones of oxidative activity in the rhizosphere
575 enhance plant roots' responses to environmental stressors, e.g., pathogens,
576 drought, and xenobiotic compounds (Muratova et al., 2009; Csiszár et al.,
577 2012; Cheeseman, 2007). They may also be important for efficient root
578 elongation and maturation (Dragišić Maksimović et al., 2008).

579 *4.5 Comparison of approaches for estimating rhizosphere extent*

580 The rhizosphere extents estimated from the zymograms depended on the
581 method used to calculate them. Use of mean + 20% activity in soil and soil

582 mean value + 2SD ('hotspot method') provided the highest and lowest
583 extents, respectively (Table 1). The hotspots of gross enzyme activity in the
584 rhizosphere estimated using the approach of Bilyera et al. (2020) occupied
585 respectively, 80 and 91.5% of the rhizosphere extents of thin (lateral) and
586 thick (seminal) roots estimated from mean soil + SD activities (Table 1). This
587 demonstrates the inhomogeneous distribution of oxidative activities, i.e., an
588 existence of "hotter" and "colder" spots, and presence of gradients within the
589 rhizosphere. The between-method differences in rhizosphere estimates
590 introduce uncertainty and preclude direct comparison of results from different
591 studies. Thus, there is a clear need for standardized methods to evaluate
592 rhizosphere size based on zymography.

593 *4.6 Effects of root traits*

594 The rhizosphere extent of oxidoreductases changed along the roots, and
595 similarly to that of hydrolytic enzymes strongly depended on root maturity and
596 radius (Fig. 6A and B; Ma et al., 2019). This clearly implies a need for
597 standardization of enzymes activities in terms of root parameters, e.g., root
598 radius and area (Ma et al., 2018) or maturity (considering contents of phenolic
599 compounds in roots) for valid comparisons (Dragišić Maksimović et al., 2008).
600 greater oxidative activity was associated with thick (seminal) roots than with
601 thin (lateral) roots, and the rhizosphere was 42% wider around them (Fig. 6C).
602 However, the normalized rhizosphere extent showed an inverse trend (Fig.
603 6D), indicating that the relative extent of oxidative processes was broader
604 around thin (lateral) roots. Thus, thin (lateral) roots might have greater
605 oxidative activity, especially peroxidase activity, per unit root area, due to

606 higher production of reactive oxygen species associated with root elongation
607 or responses to abiotic (e.g., osmotic) stress (Csiszár et al., 2012;
608 Cheeseman, 2007).

609 Moreover, cortical cells of fine roots (with < 2 mm diameter) are often
610 covered by dead cells or mycorrhizal mantel containing large amounts of
611 polyphenolic compounds (Watteau et al., 2002), which attract various
612 microbial decomposers. Greater microbial oxidative activities around roots
613 reduce the toxicity of phenolic compounds and enable their further
614 mineralization (Burke and Cairney, 2002). Thus, specific oxidative activity of
615 growing lateral (thin) roots and adjacent microbial activity resulted in greater
616 oxidative activity distributed around the lateral root as compared to seminal
617 (thick) roots. The greater apparent phenol oxidase activity in the soil than at
618 root surfaces hampered estimation of rhizosphere extents in the absence of
619 H₂O₂ in the substrate. Thus, in terms of oxidative activity, the rhizosphere
620 extents and hotspots were enzyme-specific.

621 Oxidative zymography was tested under well aerated conditions with roots
622 exposed at the front panel of the rhizoboxes. In natural soils, the activity of
623 oxidative enzymes might be affected by oxygen availability due to wide range
624 of oxidoreductases functioning under oxic and anoxic conditions in soil (Bach
625 et al., 2013; Burns et al., 2013). Temporal fluctuation in soil aeration
626 demonstrated that hydrolytic enzymes of anoxic (flooded) soils are sensitive
627 to a short-term O₂ exposure (Wang et al., 2022). In this study, we do not
628 assume strong oxidative stress during zymography performance, because the
629 whole experiment was conducted in well aerated system. However, the

630 application of oxidative zymography on paddy soils will require anaerobic
631 conditions for the whole enzymatic assay.

632 **5. Conclusions**

633 Overall, results of this study demonstrated the potential of Amplex Red-
634 based time-lapse zymography to quantify and map distributions of oxidative
635 activities. It can be simply calibrated using standard solutions of commercially
636 available resorufin. It has clear advantage over ABTS-based light adsorption
637 zymography, which lacks appropriate calibration standards (Leue et al.,
638 2021). In the Amplex Red-based assay, however, special requirements for the
639 reagent's preparation and analysis in a dark place need to be considered.

640 Four main findings were obtained with the new method. First, gross
641 oxidative activity was up to 3 times greater on the surface of maize roots than
642 on the soil surface and dominated by peroxidases. Second, peroxidase
643 activity was 26-fold lower on the soil surface than in the rhizosphere. Third,
644 gross oxidative activity decreased with distance from roots into non-
645 rhizosphere soil. Fourth, the rhizosphere extent normalized by root radius was
646 55% broader around lateral (thin) roots than around seminal (thick) roots.

647 Rhizosphere extents were strongly influenced by the estimation
648 approaches, which were only applicable for the gross oxidative activity and
649 generated varying results. Thus, the calculation of rhizosphere and hotspots
650 sizes requires standardization.

651 Relatively fast signal development and a linear relationship between the
652 signal and product content using Amplex Red-based TLZ enabled much

653 shorter zymographic monitoring (less than 15 minutes) than hydrolytic
654 zymography, thereby increasing the overall throughput of the analysis.

655 The Amplex Red-based zymography demonstrated applicability for
656 visualizing distribution of oxidative activities in maize rhizosphere and non-
657 rhizosphere area but further investigation on different plants and soil hotspots
658 is needed considering oxygen gradient in heterogeneous soil habitats.

659

660 **Declaration of interests**

661 The authors declare that they have no known competing financial interests
662 or personal relationships that could have appeared to influence the work
663 reported in this paper.

664

665 **Acknowledgement**

666 This work was done at Helmholtz-Centre for Environmental Research –
667 UFZ and financially supported by this research center. This work was
668 conducted within the framework of the priority program 2089 “Rhizosphere
669 spatiotemporal organization – a key to rhizosphere functions”, funded by the
670 Deutsche Forschungsgemeinschaft (DFG, German Research Foundation) –
671 Project number: 403664478. Seeds of the maize were provided by Caroline
672 Marcon and Frank Hochholdingner (University of Bonn). Support for this
673 research was provided in part by the USDA NIFA Program (Award # 2019-
674 67019-29361), by the NSF LTER Program (DEB 1027253) at the Kellogg
675 Biological Station, by USDA NC1187 project, by the Great Lakes Bioenergy

676 Research Center, U.S. Department of Energy, Office of Science, Office of
677 Biological and Environmental Research under Award Number DE-
678 SC0018409, by Michigan State University AgBioResearch. The first author is
679 grateful for her scholarship to Isfahan University of Technology, Isfahan, Iran.

680

681 **References**

682 Bach, C.E., Warnock, D.D., Van Horn, D.J., Weintraub, M.N., Sinsabaugh, R.L.,
683 Allison, S.D., German, D.P., 2013. Measuring phenol oxidase and
684 peroxidase activities with pyrogallol, L-DOPA, and ABTS: Effect of assay
685 conditions and soil type. *Soil Biology and Biochemistry* 67, 183-191.
686 <https://doi.org/10.1016/j.soilbio.2013.08.022>

687 Baldrian, P., 2006. Fungal laccases – occurrence and properties. *FEMS*
688 *Microbiology Reviews* 30, 215-242. 10.1111/j.1574-4976.2005.00010.x

689 Bilyera, N., Kuzyakova, I., Guber, A., Razavi, B.S., Kuzyakov, Y., 2020. How
690 “hot” are hotspots: Statistically localizing the high-activity areas on soil and
691 rhizosphere images. *Rhizosphere* 16, 100259.
692 <https://doi.org/10.1016/j.rhisph.2020.100259>

693 Bugg, T.D.H., Ahmad, M., Hardiman, E.M., Singh, R., 2011. The emerging role
694 for bacteria in lignin degradation and bio-product formation. *Current*
695 *Opinion in Biotechnology* 22, 394-400.
696 <https://doi.org/10.1016/j.copbio.2010.10.009>

697 Burke, R., Cairney, J., 2002. Laccases and other polyphenol oxidases in ecto-
698 and ericoid mycorrhizal fungi. *Mycorrhiza* 12, 105-116.
699 <https://doi.org/10.1007/s00572-002-0162-0>

700 Burns, R.G., 1982. Enzyme activity in soil: Location and a possible role in
701 microbial ecology. *Soil Biology and Biochemistry* 14, 423-427.
702 [https://doi.org/10.1016/0038-0717\(82\)90099-2](https://doi.org/10.1016/0038-0717(82)90099-2)

703 Burns, R.G., DeForest, J.L., Marxsen, J., Sinsabaugh, R.L., Stromberger, M.E.,
704 Wallenstein, M.D., Weintraub, M.N., Zoppini, A., 2013. Soil enzymes in a
705 changing environment: Current knowledge and future directions. *Soil*
706 *Biology and Biochemistry* 58, 216-234.
707 <https://doi.org/10.1016/j.soilbio.2012.11.009>

708 Cheeseman, J.M., 2007. Hydrogen peroxide and plant stress: A challenging
709 relationship. *Plant stress - Global Science Books* 1, 4-15.

710 Courty, P.E., Hoegger, P.J., Kilaru, S., Kohler, A., Buée, M., Garbaye, J.,
711 Martin, F., Kües, U., 2009. Phylogenetic analysis, genomic organization,
712 and expression analysis of multi-copper oxidases in the ectomycorrhizal
713 basidiomycete *Laccaria bicolor*. *New Phytologist* 182, 736-750.
714 <https://doi.org/10.1111/j.1469-8137.2009.02774.x>

715 Criquet, S., Joner, E., Leglize, P., Leyval, C., 2000. Anthracene and mycorrhiza
716 affect the activity of oxidoreductases in the roots and the rhizosphere of
717 lucerne (*Medicago sativa* L.). *Biotechnology Letters* 22, 1733-1737.
718 <https://doi.org/10.1023/A:1005604719909>

719 Csiszár, J., Gallé, Á., Horváth, E., Dancsó, P., Gombos, M., Váry, Z., Erdei, L.,
720 Györgyey, J., Tari, I., 2012. Different peroxidase activities and expression
721 of abiotic stress-related peroxidases in apical root segments of wheat
722 genotypes with different drought stress tolerance under osmotic stress.
723 *Plant Physiology and Biochemistry* 52, 119-129.
724 <https://doi.org/10.1016/j.plaphy.2011.12.006>

725 Dennis, P.G., Miller, A.J., Hirsch, P.R., 2010. Are root exudates more important
726 than other sources of rhizodeposits in structuring rhizosphere bacterial
727 communities? *FEMS Microbiology Ecology* 72, 313-327.
728 <https://doi.org/10.1111/j.1574-6941.2010.00860.x>

729 Dragišić Maksimović, J., Maksimović, V., Živanović, B., Hadži-Tašković
730 Šukalović, V., Vuletić, M., 2008. Peroxidase activity and phenolic
731 compounds content in maize root and leaf apoplast, and their association
732 with growth. *Plant Science* 175, 656-662.
733 <https://doi.org/10.1016/j.plantsci.2008.06.015>

734 Driever, S.M., Fryer, M.J., Mullineaux, P.M., Baker, N.R., 2009. Imaging of
735 Reactive Oxygen Species In vivo, In: Pfannschmidt, T. (Eds.), *Plant Signal*
736 *Transduction: Methods and Protocols*. Humana Press, Totowa, NJ, pp.
737 109-116. https://doi.org/10.1007/978-1-59745-289-2_7

738 Dwivedi, D., Tang, J., Bouskill, N., Georgiou, K., Chacon, S.S., Riley, W.J.,
739 2019. Abiotic and biotic controls on soil organo–mineral interactions:
740 Developing model structures to analyze why soil organic matter persists.
741 *Reviews in Mineralogy and Geochemistry* 85, 329-348.
742 <https://doi.org/10.2138/rmg.2019.85.11>

743 German, D.P., Weintraub, M.N., Grandy, A.S., Lauber, C.L., Rinkes, Z.L.,
744 Allison, S.D., 2011. Optimization of hydrolytic and oxidative enzyme
745 methods for ecosystem studies. *Soil Biology and Biochemistry* 43, 1387-
746 1397. <https://doi.org/10.1016/j.soilbio.2011.03.017>

747 Gramss, G., Voigt, K.D., Kirsche, B., 1999. Oxidoreductase enzymes liberated
748 by plant roots and their effects on soil humic material. *Chemosphere* 38,
749 1481-1494. [https://doi.org/10.1016/S0045-6535\(98\)00369-5](https://doi.org/10.1016/S0045-6535(98)00369-5)

750 Guber, A., Blagodatskaya, E., Juyal, A., Razavi, B.S., Kuzyakov, Y.,
751 Kravchenko, A., 2021. Time-lapse approach to correct deficiencies of 2D
752 soil zymography. *Soil Biology and Biochemistry* 157, 108225.
753 <https://doi.org/10.1016/j.soilbio.2021.108225>

754 Guber, A., Kravchenko, A., Razavi, B.S., Uteau, D., Peth, S., Blagodatskaya,
755 E., Kuzyakov, Y., 2018. Quantitative soil zymography: Mechanisms,
756 processes of substrate and enzyme diffusion in porous media. *Soil Biology*
757 *and Biochemistry* 127, 156-167.
758 <https://doi.org/10.1016/j.soilbio.2018.09.030>

759 Guber, A.K., Kravchenko, A.N., Razavi, B.S., Blagodatskaya, E., Kuzyakov, Y.,
760 2019. Calibration of 2-D soil zymography for correct analysis of enzyme
761 distribution. *European Journal of Soil Science* 70, 715-726.
762 <https://doi.org/10.1111/ejss.12744>

763 Hinsinger, P., Bengough, A.G., Vetterlein, D., Young, I.M., 2009. Rhizosphere:
764 biophysics, biogeochemistry and ecological relevance. *Plant and Soil* 321,
765 117-152. <https://doi.org/10.1007/s11104-008-9885-9>

766 Hoang, D.T.T., Razavi, B.S., Kuzyakov, Y., Blagodatskaya, E., 2016.
767 Earthworm burrows: Kinetics and spatial distribution of enzymes of C-, N-
768 and P- cycles. *Soil Biology and Biochemistry* 99, 94-103.
769 <https://doi.org/10.1016/j.soilbio.2016.04.021>

770 Hochholdinger, F., 2009. The Maize Root System: Morphology, Anatomy, and
771 Genetics, In: Bennetzen, J.L., Hake, S.C. (Eds.), *Handbook of Maize: Its*
772 *Biology*. Springer New York, New York, NY, pp. 145-160. 10.1007/978-0-
773 387-79418-1_8

774 Huang, A., Wang, Y., Liu, Y., Wang, G., She, X., 2020. Reactive oxygen
775 species regulate auxin levels to mediate adventitious root induction in
776 *Arabidopsis* hypocotyl cuttings. *Journal of Integrative Plant Biology* 62, 912-
777 926. <https://doi.org/10.1111/jipb.12870>

778 Hummel, C., Boitt, G., Santner, J., Lehto, N.J., Condrón, L., Wenzel, W.W.,
779 2021. Co-occurring increased phosphatase activity and labile P depletion
780 in the rhizosphere of *Lupinus angustifolius* assessed with a novel,
781 combined 2D-imaging approach. *Soil Biology and Biochemistry* 153,
782 107963. <https://doi.org/10.1016/j.soilbio.2020.107963>

783 Kováčik, J., Babula, P., Klejdus, B., Hedbavny, J., Jarošová, M., 2014.
784 Unexpected behavior of some nitric oxide modulators under cadmium
785 excess in plant tissue. *PLoS ONE* 9, e91685.
786 <https://doi.org/10.1371/journal.pone.0091685>

787 Kuzyakov, Y., 2002. Review: Factors affecting rhizosphere priming effects.
788 *Journal of Plant Nutrition and Soil Science* 165, 382-396.
789 [https://doi.org/10.1002/1522-2624\(200208\)165:4<382::aid-
790 jpln382>3.0.co;2-#](https://doi.org/10.1002/1522-2624(200208)165:4<382::aid-jpln382>3.0.co;2-#)

791 Kuzyakov, Y., Razavi, B.S., 2019. Rhizosphere size and shape: Temporal
792 dynamics and spatial stationarity. *Soil Biology and Biochemistry* 135, 343-
793 360. <https://doi.org/10.1016/j.soilbio.2019.05.011>

794 Lefrançois, P., Vajjala, V.S.R., Arredondo, I.B., Goudeau, B., Doneux, T.,
795 Bouffier, L., Arbault, S., 2016. Direct oxidative pathway from amplex red to
796 resorufin revealed by in situ confocal imaging. *Physical Chemistry
797 Chemical Physics* 18, 25817-25822. <https://doi.org/10.1039/C6CP04438G>

798 Leue, M., Holz, M., Gerke, H.H., Taube, R., Puppe, D., Wirth, S., 2021.
799 Spatially-distributed microbial enzyme activities at intact, coated macropore
800 surfaces in Luvisol Bt-horizons. *Soil Biology and Biochemistry* 156, 108193.
801 <https://doi.org/10.1016/j.soilbio.2021.108193>

802 Loepmann, S., Blagodatskaya, E., Pausch, J., Kuzyakov, Y., 2016. Substrate
803 quality affects kinetics and catalytic efficiency of exo-enzymes in
804 rhizosphere and detritosphere. *Soil Biology and Biochemistry* 92, 111-118.
805 <https://doi.org/10.1016/j.soilbio.2015.09.020>

806 Ma, X., Mason-Jones, K., Liu, Y., Blagodatskaya, E., Kuzyakov, Y., Guber, A.,
807 Dippold, M.A., Razavi, B.S., 2019. Coupling zymography with pH mapping
808 reveals a shift in lupine phosphorus acquisition strategy driven by cluster
809 roots. *Soil Biology and Biochemistry* 135, 420-428.
810 <https://doi.org/10.1016/j.soilbio.2019.06.001>

811 Ma, X., Zarebanadkouki, M., Kuzyakov, Y., Blagodatskaya, E., Pausch, J.,
812 Razavi, B.S., 2018. Spatial patterns of enzyme activities in the rhizosphere:
813 Effects of root hairs and root radius. *Soil Biology and Biochemistry* 118, 69-
814 78. <https://doi.org/10.1016/j.soilbio.2017.12.009>

815 Muratova, A., Pozdnyakova, N., Golubev, S., Wittenmayer, L., Makarov, O.,
816 Merbach, W., Turkovskaya, O., 2009. Oxidoreductase activity of sorghum
817 root exudates in a phenanthrene-contaminated environment.
818 *Chemosphere* 74, 1031-1036.
819 <https://doi.org/10.1016/j.chemosphere.2008.11.011>

820 Nannipieri, P., Kandeler, E., Ruggiero, P., 2002. Enzyme activities and
821 microbiological and biochemical processes in soil, In: Richard G. Burns,

822 R.P.D. (Eds.), *Enzymes in the Environment: Activity, Ecology, and*
823 *Applications*, 2 ed. Marcel Dekker Inc., New York. Basel, pp. 1 - 35.

824 R Development Core Team, 2020. R: A language and environment for
825 statistical computing. R Development Core Team, Vienna, Austria.
826 <https://www.r-project.org>

827 Razavi, B.S., Zhang, X., Bilyera, N., Guber, A., Zarebanadkouki, M., 2019. Soil
828 zymography: Simple and reliable? Review of current knowledge and
829 optimization of the method. *Rhizosphere* 11, 100161.
830 <https://doi.org/10.1016/j.rhisph.2019.100161>

831 Reszka, K.J., Wagner, B.A., Burns, C.P., Britigan, B.E., 2005. Effects of
832 peroxidase substrates on the Amplex red/peroxidase assay: Antioxidant
833 properties of anthracyclines. *Analytical Biochemistry* 342, 327-337.
834 <https://doi.org/10.1016/j.ab.2005.04.017>

835 Sanaullah, M., Razavi, B.S., Blagodatskaya, E., Kuzyakov, Y., 2016. Spatial
836 distribution and catalytic mechanisms of β -glucosidase activity at the root-
837 soil interface. *Biology and Fertility of Soils* 52, 505-514.
838 <https://doi.org/10.1007/s00374-016-1094-8>

839 SAS Institute, 2013. *SAS Procedures Guide*, 9.4., ed. SAS Institute Inc., Cary,
840 NC.

841 Schindelin, J., Arganda-Carreras, I., Frise, E., Kaynig, V., Longair, M., Pietzsch,
842 T., Preibisch, S., Rueden, C., Saalfeld, S., Schmid, B., Tinevez, J.-Y.,
843 White, D.J., Hartenstein, V., Eliceiri, K., Tomancak, P., Cardona, A., 2012.
844 Fiji: An open-source platform for biological-image analysis. *Nature Methods*
845 9, 676-682. <https://doi.org/10.1038/nmeth.2019>

846 Shah, F., Nicolás, C., Bentzer, J., Ellström, M., Smits, M., Rineau, F., Canbäck,
847 B., Floudas, D., Carleer, R., Lackner, G., Braesel, J., Hoffmeister, D.,
848 Henrissat, B., Ahrén, D., Johansson, T., Hibbett, D.S., Martin, F., Persson,
849 P., Tunlid, A., 2016. Ectomycorrhizal fungi decompose soil organic matter
850 using oxidative mechanisms adapted from saprotrophic ancestors. *New*
851 *Phytologist* 209, 1705-1719. <https://doi.org/10.1111/nph.13722>

852 Sinsabaugh, R.L., 2010. Phenol oxidase, peroxidase and organic matter
853 dynamics of soil. *Soil Biology and Biochemistry* 42, 391-404.
854 <https://doi.org/10.1016/j.soilbio.2009.10.014>

855 Spohn, M., Carminati, A., Kuzyakov, Y., 2013. Soil zymography – A novel in
856 situ method for mapping distribution of enzyme activity in soil. *Soil Biology*
857 *and Biochemistry* 58, 275-280.
858 <https://doi.org/10.1016/j.soilbio.2012.12.004>

859 Spohn, M., Kuzyakov, Y., 2013. Distribution of microbial- and root-derived
860 phosphatase activities in the rhizosphere depending on P availability and C
861 allocation – Coupling soil zymography with ¹⁴C imaging. *Soil Biology and*
862 *Biochemistry* 67, 106-113. <https://doi.org/10.1016/j.soilbio.2013.08.015>

863 Tang, J., Wang, W., Yang, L., Cao, C., Li, X., 2019. Variation in quantity and
864 chemical composition of soil dissolved organic matter in a peri-urban critical
865 zone observatory watershed in Eastern China. *Science of The Total*
866 *Environment* 688, 622-631. <https://doi.org/10.1016/j.scitotenv.2019.06.270>

867 Theuerl, S., Buscot, F., 2010. Laccases: Toward disentangling their diversity
868 and functions in relation to soil organic matter cycling. *Biology and Fertility*
869 *of Soils* 46, 215-225. <https://doi.org/10.1007/s00374-010-0440-5>

870 Tuomela, M., Hatakka, A., 2011. 6.16 - Oxidative fungal enzymes for
871 bioremediation, In: Moo-Young, M. (Eds.), *Comprehensive Biotechnology*
872 (Second Edition). Academic Press, Burlington, pp. 183-196.
873 <https://doi.org/10.1016/B978-0-08-088504-9.00370-6>

874 Vetterlein, D., Lippold, E., Schreiter, S., Phalempin, M., Fahrenkamp, T.,
875 Hochholding, F., Marcon, C., Tarkka, M., Oburger, E., Ahmed, M.,
876 Javaux, M., Schlüter, S., 2021. Experimental platforms for the investigation
877 of spatiotemporal patterns in the rhizosphere—Laboratory and field scale.
878 *Journal of Plant Nutrition and Soil Science* 184, 35-50.
879 <https://doi.org/10.1002/jpln.202000079>

880 Voothuluru, P., Braun, D.M., Boyer, J.S., 2018. An in vivo imaging assay
881 detects spatial variability in glucose release from plant roots. *Plant*
882 *Physiology* 178, 1002-1010. <https://doi.org/10.1104/pp.18.00614>

883 Wang, C., Dippold, M.A., Blagodatskaya, E., Dorodnikov, M., 2022. Oxygen
884 matters: Short- and medium-term effects of aeration on hydrolytic enzymes
885 in a paddy soil. *Geoderma* 407, 115548.
886 <https://doi.org/10.1016/j.geoderma.2021.115548>

887 Wang, T., Xiang, Y., Liu, X., Chen, W., Hu, Y., 2017. A novel fluorimetric method
888 for laccase activities measurement using Amplex Red as substrate. *Talanta*
889 162, 143-150. <https://doi.org/10.1016/j.talanta.2016.10.006>

890 Watteau, F., Villemin, G., Ghanbaja, J., Genet, P., Pargney, J.-C., 2002. In situ
891 ageing of fine beech roots (*Fagus sylvatica*) assessed by transmission
892 electron microscopy and electron energy loss spectroscopy: Description of
893 microsites and evolution of polyphenolic substances. *Biology of the Cell* 94,
894 55-63. [https://doi.org/10.1016/S0248-4900\(02\)01182-6](https://doi.org/10.1016/S0248-4900(02)01182-6)

895 Zhao, B., Rangelova, K., Jiang, J., Mason, R.P., 2011. Studies on the
896 photosensitized reduction of resorufin and implications for the detection of
897 oxidative stress with Amplex Red. *Free Radical Biology and Medicine* 51,
898 153-159. <https://doi.org/10.1016/j.freeradbiomed.2011.03.016>

899 Zhao, B., Summers, F.A., Mason, R.P., 2012. Photooxidation of Amplex red to
900 resorufin: Implications of exposing the Amplex red assay to light. *Free*
901 *Radical Biology and Medicine* 53, 1080-1087.
902 <https://doi.org/10.1016/j.freeradbiomed.2012.06.034>

903 Zhu, B., Gutknecht, J.L.M., Herman, D.J., Keck, D.C., Firestone, M.K., Cheng,
904 W., 2014. Rhizosphere priming effects on soil carbon and nitrogen
905 mineralization. *Soil Biology and Biochemistry* 76, 183-192.
906 <https://doi.org/10.1016/j.soilbio.2014.04.033>

907

908

909

910

911

912

913

914

915

916

917 **Table 1** Comparison of methods for estimating the rhizosphere extent and
 918 hotspot areas applied to the same set of thick (seminal) and thin (lateral)
 919 maize roots.

Methods	Authors	Method description	Rhizosphere extent/hotspot size, mm	
			Thick root (seminal)	Thin root (lateral)
The rhizosphere extent of enzyme activity				
Soil mean value + 20%	Ma et al. (2019)	The distance from the center of root to the region where the enzyme activity is at least 20% greater than in the bulk soil.	1.40 (0.05)*	0.90 (0.09)
Soil mean value + 30%	Ma et al. (2018)	The distance from the center of root to the region where the enzyme activity is at least 30% greater than in the bulk soil.	1.38 (0.02)	0.89 (0.08)
Soil mean value + SD		The distance from the center of root to the region where the enzyme activity is greater than the mean value + SD in the bulk soil	1.26 (0.15)	0.73 (0.17)
The hotspot area of enzyme activity				
Hotspots (Mean+2SD)	Bilyera et al. (2020)	A normal distribution is fitted to the left (low greyscale values) part of the whole greyscale histogram and defined as background enzyme activity. Hotspot areas are defined by applying a mean+2SD threshold to activity images.	1.16 (0.13)	0.63 (0.13)

920 * Standard deviation (Std)

921

922

923

924

925 **FIGURE CAPTIONS**

926 **Fig. 1.** Schematic illustration of rhizosphere extents (A) and hotspots (B)
927 estimated using methods listed in Table 1.

928 **Fig. 2.** Calibration and validation of zymography images based on resorufin
929 amount applied to the membrane. $\Sigma G \times F$ denotes sums of greyscale values
930 (GSVs) in images of calibration and validation membranes with indicated
931 amounts of resorufin.

932 **Fig. 3.** Illustrative examples of grey scale value (GSV) dynamics of
933 oxidative zymograms obtained with (filled symbols) and without (empty
934 symbols) H_2O_2 in the substrate. Error bars indicate standard deviation of
935 GSVs recorded in two sets of zymograms in three replicates.

936 **Fig. 4.** An example of zymogram of gross peroxidase and phenol oxidase
937 (A); and phenol oxidase (B) activities during the 0–15 min (a) and 30–90 min
938 (b) zymography time intervals. Daylight photos of soil-root surfaces of maize
939 (*Zea mays* L.) are shown in the (c) panels. The green lines represent root
940 locations. The yellow and blue dashed rectangles mark areas with an
941 example of good attachment selected for thin (lateral) and thick (seminal)
942 roots, respectively. The red dashed rectangles show root areas with an
943 example of bad attachment. The root photos were taken after TLZ.

944 **Fig. 5.** Mean gross oxidative (Total), phenol oxidase, and peroxidase
945 activities at the maize root and soil surfaces during two zymography time
946 intervals. Different lowercase letters (a, b) indicate significant differences ($P <$
947 0.05) between root and soil within the two time intervals. Error bars indicate
948 one standard deviation of the rhizosphere extents.

949 **Fig. 6.** Gross oxidative activity decreasing with distance from thick
950 (seminal; A) and thin (lateral; B) roots. Each line represents the selected root
951 mean values of three zymograms (n=3). Error bars of oxidative activities have
952 been omitted to improve visualization. Mean values of the rhizosphere extent
953 (RE) of gross oxidative activity of maize thick (seminal) and thin (lateral) roots
954 (C), and rhizosphere extent normalized by root radius (D). Different lowercase
955 letters (a, b) indicate significant differences ($P < 0.05$) in rhizosphere extent
956 between thick (seminal) and thin (lateral) roots. Error bars indicate standard
957 deviation of the rhizosphere extents.

958

959

960

961

962

963

964

965

966

967

968

969

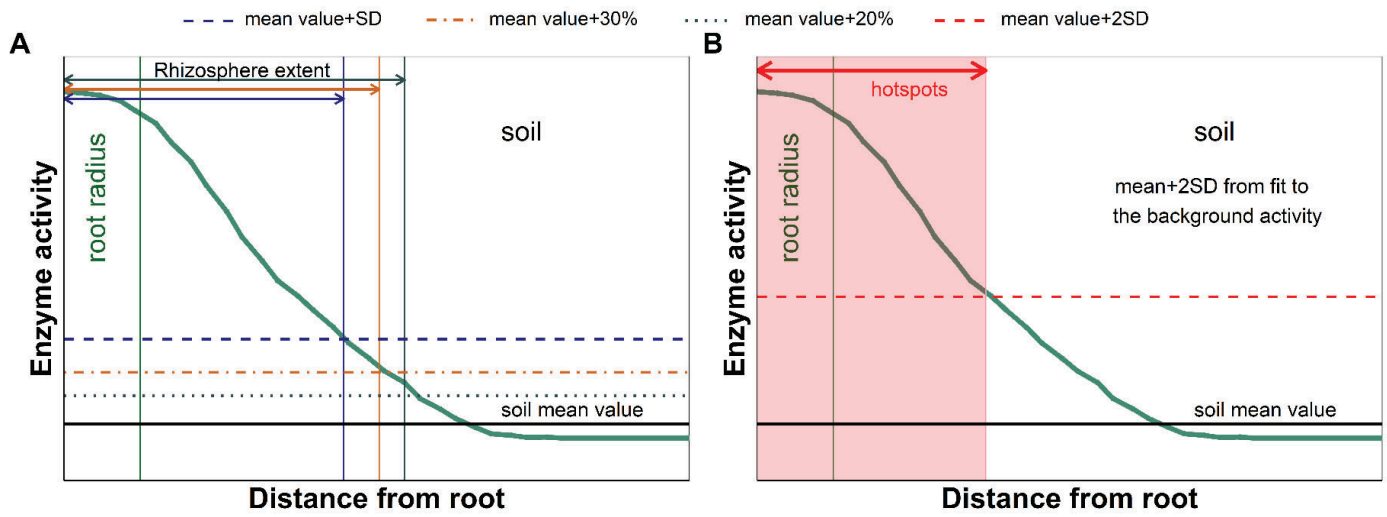
970

971

972

973

974 **Fig. 1.**



976

977

978

979

980

981

982

983

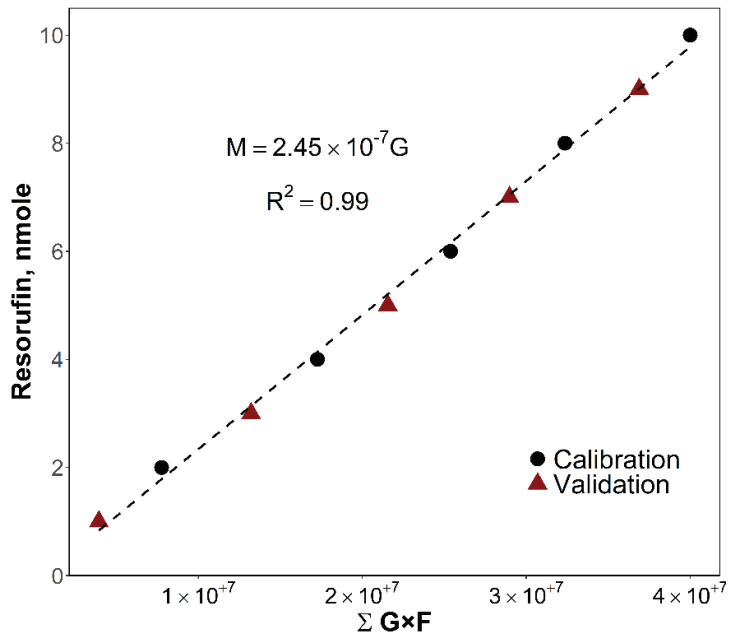
984

985

986

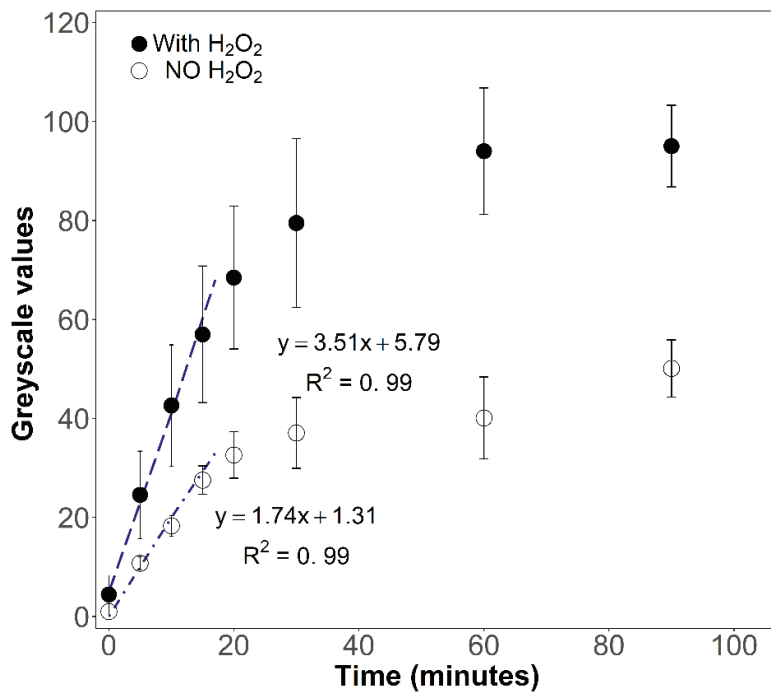
987

988 Fig. 2.



989

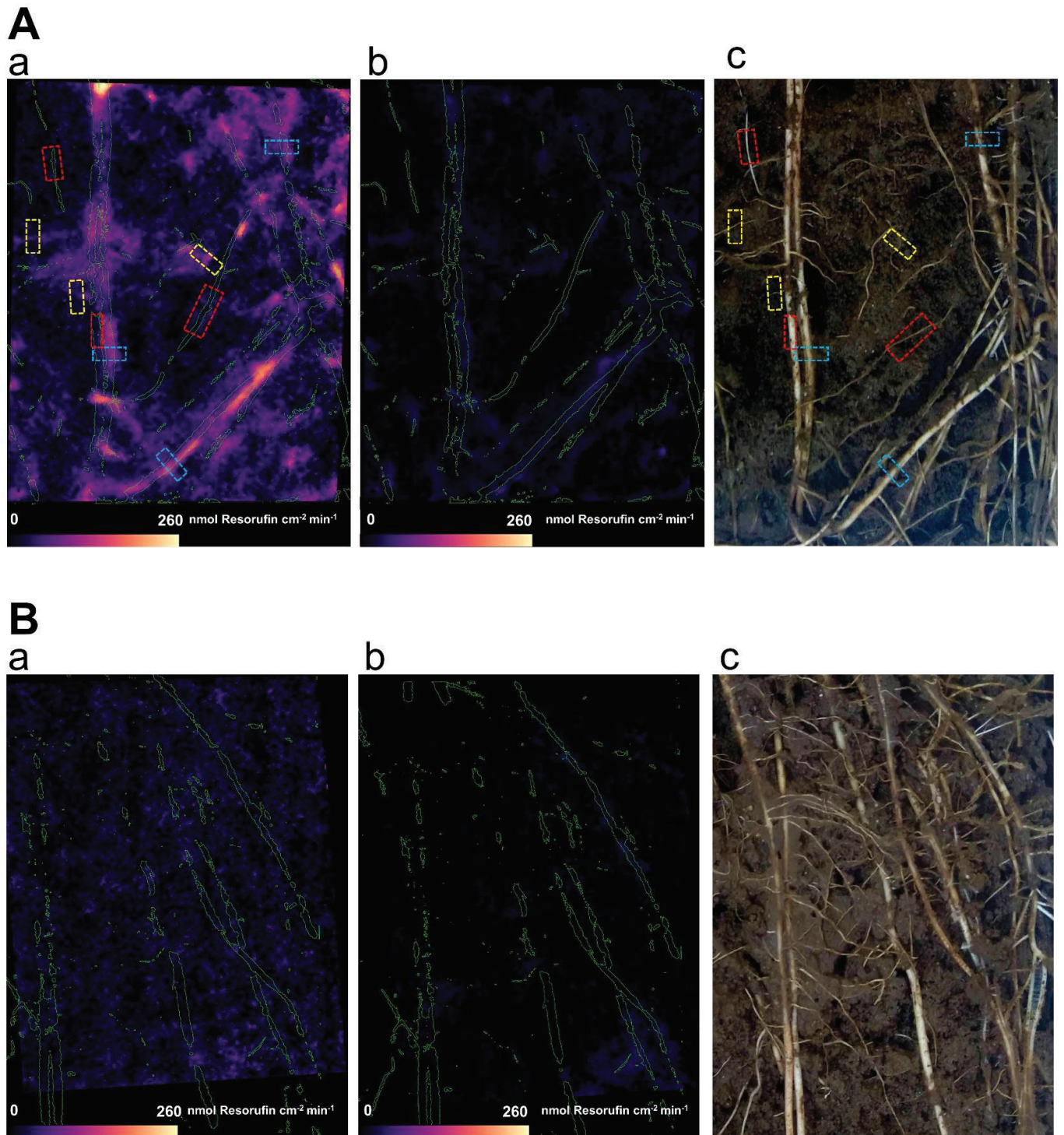
990 Fig. 3.



991

992

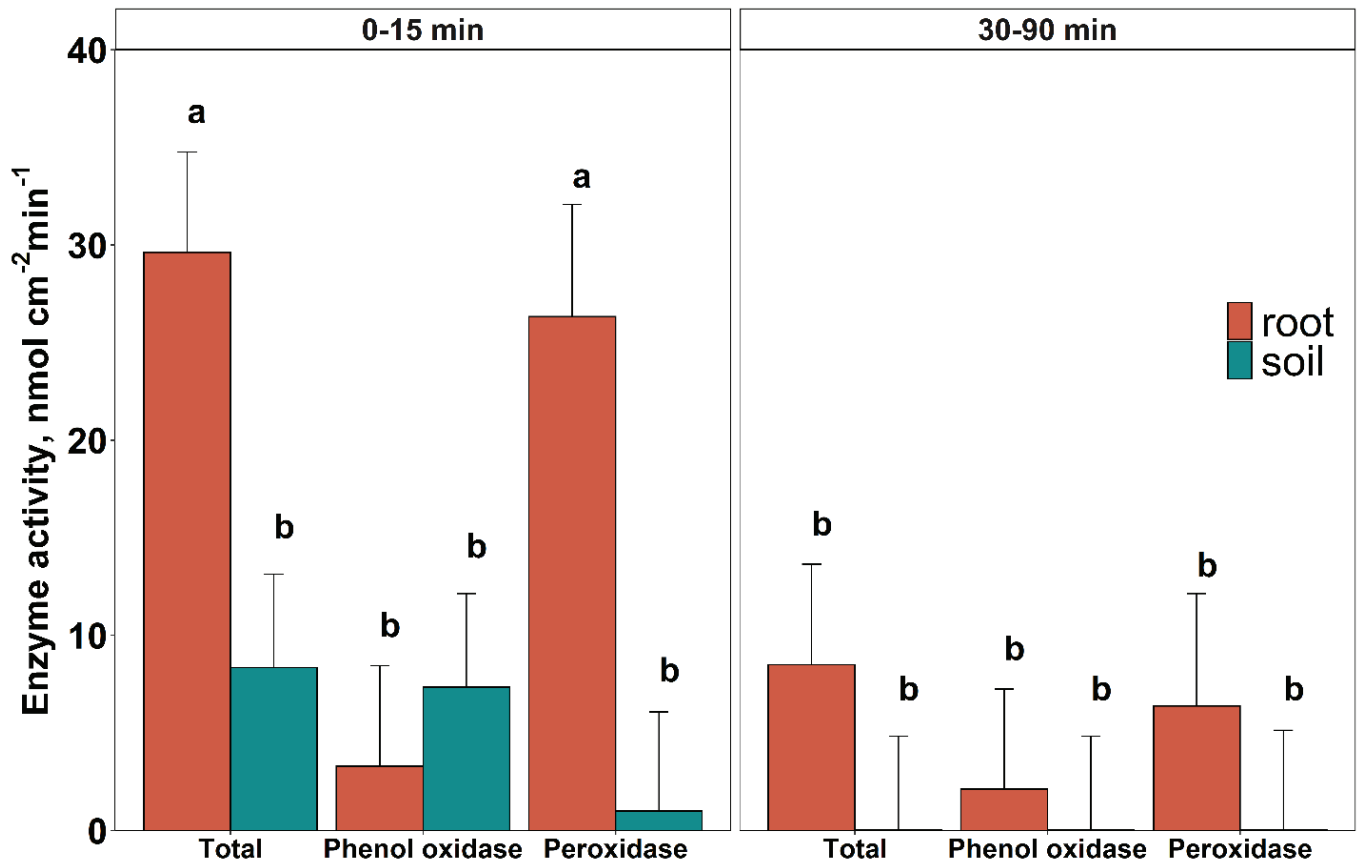
993



997

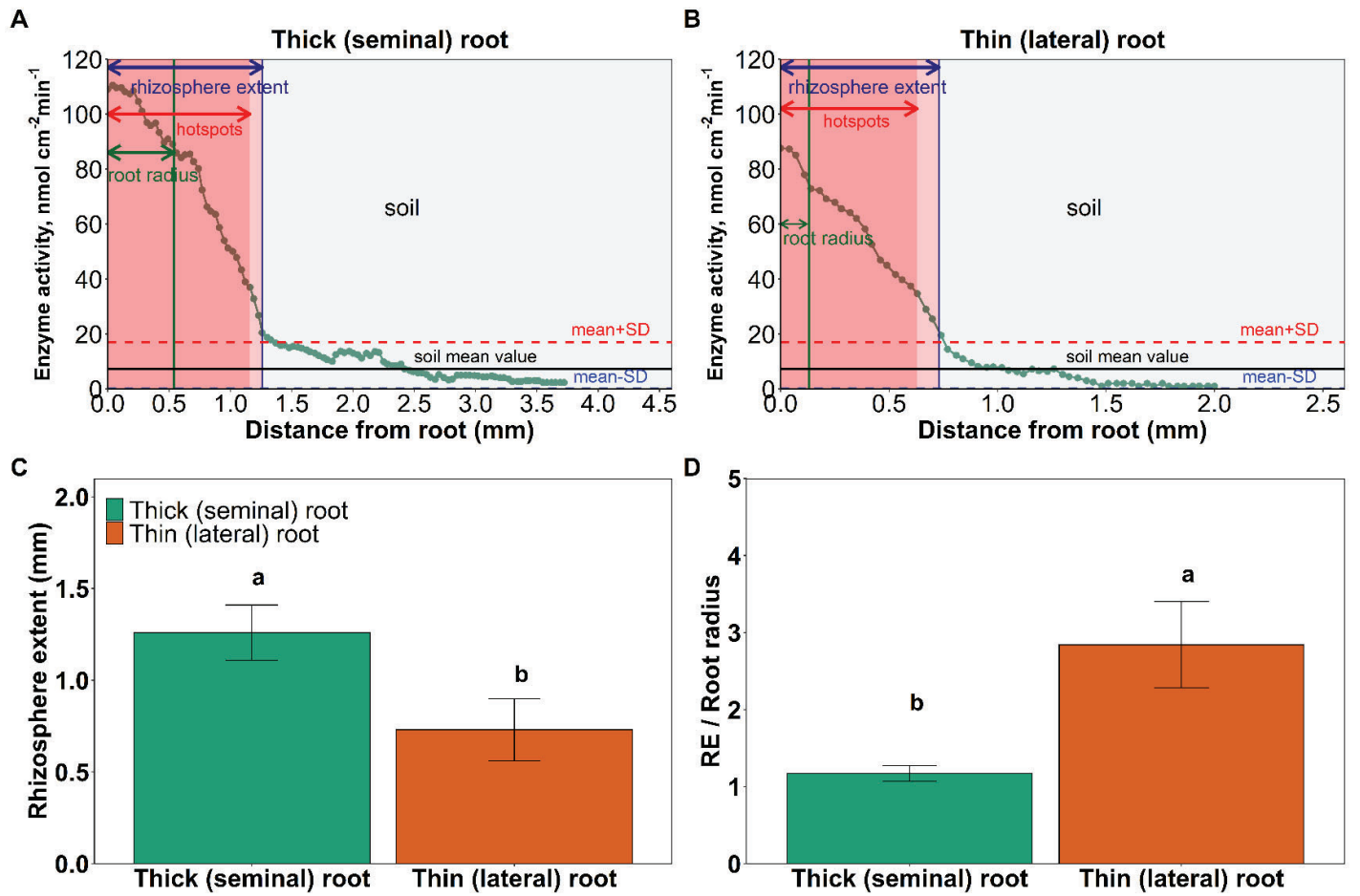
998

999 Fig. 5.



1001
1002
1003
1004
1005
1006
1007
1008
1009
1010
1011
1012
1013

1014 **Fig. 6.**



1016

1017

1018

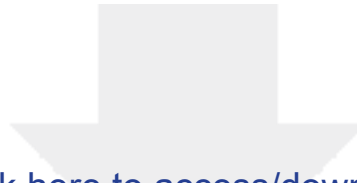
1019

1020

1021

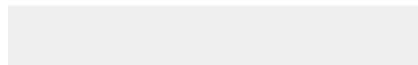
1022

1023



Click here to access/download

Supplementary Material for online publication only
Supplementary_oxidative zymography.docx



Declaration of interests

The authors declare that they have no known competing financial interests or personal relationships that could have appeared to influence the work reported in this paper.